Augmentation of Paramedian 3D Ultrasound Images of the Spine

Abtin Rasoulian[1], Robert N. Rohling[1,2], and Purang Abolmaesumi[1]

[1] Department of Electrical and Computer Engineering
[2] Department of Mechanical Engineering,
University of British Columbia, Vancouver, B.C., Canada
{abtinr,rohling,purang}@ece.ubc.ca

Abstract. The blind placement of an epidural needle is among the most difficult regional anesthetic techniques. The challenge is to insert the needle in the mid-sagittal plane and to avoid overshooting the needle into the spinal cord. Prepuncture 2D ultrasound scanning has been introduced as a reliable tool to localize the target and facilitate epidural needle placement. Ideally, real-time ultrasound should be used *during* needle insertion. However, several issues inhibit the use of standard 2D ultrasound, including the obstruction of the puncture site by the ultrasound probe, low visibility of the target in ultrasound images, and increased pain due to longer needle trajectory. An alternative is to use 3D ultrasound imaging, where the needle and target could be visible within the same reslice of a 3D volume; however, novice ultrasound users (i.e., many anesthesiologists) still have difficulty interpreting ultrasound images of the spine and identifying the target epidural space. In this paper, we propose to augment 3D ultrasound images by registering a multi-vertebrae statistical shape+pose model. We use such augmentation for enhanced interpretation of the ultrasound and identification of the mid-sagittal plane for the needle insertion. Validation is performed on synthetic data derived from the CT images, and 64 *in vivo* ultrasound volumes.

Keywords: multi-vertebrae shape+pose model, 3D ultrasound, Gaussian mixture model-based registration.

1 Introduction

Epidurals are a form of regional anesthesia commonly used in obstetrics during labour and delivery, and they are effective alternatives to general anesthesia for cesarean delivery. Epidurals involve the insertion of a needle between the vertebrae into a space called the epidural space (see Fig. 1a). The use of epidurals has increased over the past few decades but conventional epidural techniques continue to have a failure rate in the range of 6-20% [4], meaning the patient has inadequate or no pain relief.

Before the procedure, no detailed knowledge about the individual patient's spinal anatomy is available to guide the anesthesiologist. Therefor, epidurals are traditionally guided by palpation of surface landmarks to identify an appropriate intervertebral space and to select a skin puncture site along the midline of

D. Barratt et al. (Eds.): IPCAI 2013, LNCS 7915, pp. 51–60, 2013.

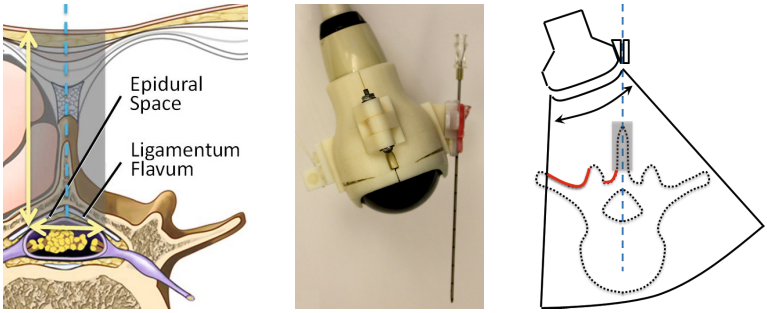

Fig. 1. a) Midline sagittal insertion of the needle. The horizontal arrow shows the epidural width and the vertical arrow shows the epidural depth. b) 3D motorized ultrasound probe equipped with a needle guide. c) The relative positions of the 3D ultrasound probe, needle and vertebra in superior-inferior view. The arrow shows the sweep direction. The probe should be placed to align the needle path (dashed blue line) with the mid-sagittal plane. The red line shows the visible part of the vertebrae in ultrasound images. No echoes appear on the gray area since the spinous process surface is not orthogonal to the transducer.

the spine. The loss-of-resistance technique is normally used to confirm that the needle tip has reached the epidural space. This technique involves attaching a saline-filled syringe to the needle and applying pressure during needle insertion and then feeling the loss-of-resistance to saline injection when the needle tip enters the epidural space. The most common complication (0.5% to 2.5% [16]) arises from overshoot and accidental puncture of the dura mater surrounding the spinal cord and leakage of cerebral spinal fluid, which leads to side effects for patients, such as post dural puncture headache.

To reduce complications, ultrasound imaging has been proposed since it poses no known risk to the patient, making it the only modality that is feasible for obstetric anesthesiology. 2D ultrasound imaging has been demonstrated as a pre-puncture tool for measuring the distance from the skin to the epidural space (referred to as the epidural depth) and to help decide the puncture site [8].

Ideally, ultrasound would also be used *during* needle insertion to visually confirm the needle progressing toward and then entering the epidural space correctly. Unfortunately, real-time guidance of a midline needle insertion is hindered by the fact that a standard 2D ultrasound transducer obscures the puncture site, and moving the transducer to the side makes it impossible to view both the needle tip and the target together. The usual image-guidance solutions based on tracking of both the needle and the ultrasound transducer do not work in this application. The tracking sensor would need to be either mounted on the base of the needle, which reduces the accuracy due to needle bending, or placed inside the needle close to its tip, which prohibits the standard procedure of loss-of-resistance since the sensor does not allow passage of the saline.

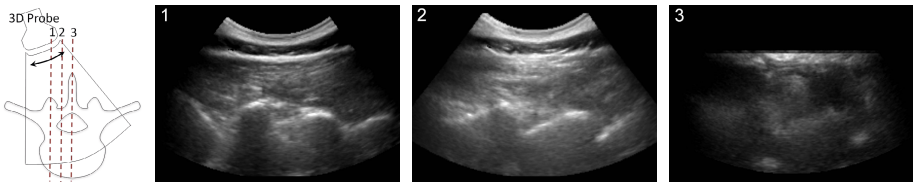

Fig. 2. Three parallel slices extracted from the 3D ultrasound image. Arrow shows the sweep direction. Planes are spaced 10 mm from each other. Ideally, the anesthesiologist should perform the needle injection in the third plane which does not include strong features. The first plane shows the facet joints whereas the second plane shows the laminae. The planes are also hard for novice users to distinguish the anatomy in the ultrasound, making needle guidance difficult.

A solution to these problems has been developed using a 3D motorized ultrasound transducer equipped with a needle guide (see Figure 1b and 1c) [13]. 3D ultrasound is widely used in obstetrics and has several advantages such as easier diagnosis of cleft palate [17]. 3D ultrasound also has the potential to improve epidural catheterization and operation orientation of the vertebral column [1]. In our solution, a virtual anterior-posterior plane (hereafter referred to as a reslice plane) containing the needle path is extracted from volumes captured in real time by the transducer. Placing the transducer in a paramedian plane and consequently placing the needle in midline, the reslice plane depicts both the needle and the epidural space. Initial experiments on animals have shown the feasibility of this approach [13], but there are still limitations of this technique. First, the ultrasound images are hard to interpret and require extensive training. Second, detection of the mid-sagittal plane is not trivial due to a lack of significant image features in this plane (see Fig. 2).

In the absence of pre-operative CT image for the majority of obstetric cases, augmentation of 3D ultrasound has been explored previously by registering a statistical shape model of a single vertebra [15]. In that study, the ultrasound volumes were acquired with the probe centered on the midline and bony features from both side of the vertebrae were visible. In this paper we modify that approach and make two main contributions. First, we demonstrate construction of the multi-vertebrae shape+pose statistical model and its registration to ultrasound volumes of the spine. Second, we perform the registration to single-sided paramedian ultrasound volumes. Registration is challenging due to the lack of echoes on the contra-lateral side, and thus a lack of information on the symmetric shape of the vertebrae.

In summary, the model is registered to the ultrasound images based on echoes that are typically visible in such ultrasound images, i.e. laminae, articular processes, and transverse processes of one side of the vertebrae. We use the registered model to interpret the echoes in the ultrasound images and to predict the mid-sagittal plane. We validate our registration technique on synthetic data and 64 *in vivo* ultrasound volumes.

2 Methods

2.1 Construction of the Multi-vertebrae Model

Several techniques have been proposed for construction of multi-object statistical models [2,9,5,10,12]. In some of these techniques, the pose statistics are neglected by implicitly representing them in the shape statistics. This representation leads to two major issues: first, the pose statistics are not necessarily correlated with the shape statistics, since they depend on external factors such as the position and orientation of the patient during data acquisition. Second, the shape deformations are assumed to lie on a Euclidean space. On the other hand, the poses are represented by similarity transformations, i.e. rigid+scale transformations. These transformations form a Lie group, which is a Riemannian manifold where analysis performed in Euclidean space is not applicable [6]. To address this problem, we adapt a technique proposed by Bossa and Olmos [2] to generate a statistical multi-vertebrae shape+pose model.

A Lie group G is a group and a differentiable manifold where multiplication and inversion are smooth. The tangent space at the identity element is called Lie algebra, $\mathfrak{g}$. The exponential mapping, $\mathfrak{g} : \exp(x) \rightarrow G$, and its inverse, logarithm mapping $G : \log(x) \rightarrow \mathfrak{g}$, are used to map elements in the tangent space into G and vice versa.

Analogous to principal components in the Euclidean space, Principal Geodesics (PG), are defined for Lie groups. The approximation as suggested By Fletcher *et al.* [6] is as follows: for a set of elements, $x_1, \ldots, x_n$, the mean, μ, is found using an iterative approach. Principal Component Analysis (PCA) is then applied to the residuals in the Lie algebra, $\log(\mu^{-1}x_i)$. The results are orthonormal principal components, v_l, which give the PGs by exponential mapping, $\mu \exp(v_l)$.

Assume that the training set contains N instances of an ensemble of L anatomies (in this case L vertebrae), each represented by a point set as its boundary. Initially, a group-wise Gaussian mixture model (GMM)-based registration technique [14] is used to establish dense correspondences across the training set. Generalized Procrustes analysis is then used to generate the mean shape for all the anatomies, and their transformation, $\mathbf{T}_{n,l}$, to each instance. The transformation, $\mathbf{T}_{n,l}$, is the similarity transformation from the lth anatomy of the mean shape to the corresponding anatomy of the nth instance. The transformation for all anatomies are concatenated and PGs are then extracted. The results are principal geodesics, which can separately be written for each anatomy: $\mu_l^p \exp(\mathbf{v}_{k,l}^p)$. Shapes also form a Lie group [2] and similarly shapes' PGs can be represented by $\mu_l^s \exp(\mathbf{v}_{k,l}^s)$. Note that we use superscript "s" and "p" to differentiate between shape and pose related variables, respectively.

2.2 Enhancement of the Ultrasound Images

A preprocessing step is performed on the ultrasound images to extract the bone surface probability using high intensity and shadow information. To extract the

bone surface probability, we use an adaptation of a technique proposed by Foroughi *et al.* [7]. Initially, the image is filtered by Laplace of Gaussian (LoG) kernel to extract the high intensity pixels which typically have larger probability to be on the bone surface. The result is added to the blurred image. Next, the blurred image is convoluted by a profile highlighting the shadow beneath a pixel. The shadow image is combined with the blurred image to generate the bone probability map.

2.3 Registration of the Model to the Ultrasound Images

The multi-object statistical model can be instantiated by applying different weights to the PGs and combining them. Assuming that w_k^s is the weight applied to the kth shape PG and w_k^p is applied to the kth pose PG, the lth object of the model can be instantiated as follows:

$$s_l = \Phi(\mathbf{w}^s, \mathbf{w}^p) = \Phi_l^p\big(\Phi_l^s(\mathbf{w}^s); \mathbf{w}^p\big), \tag{1}$$

where $\Phi_l^p(.; \mathbf{w}^p)$ and $\Phi_l^s(.)$ denote a similarity transformation and a shape, respectively, which are built by a combination of the pose and shape PGs with corresponding weights:

$$\Phi^p(.; \mathbf{w}^p) = \mu_l^p \prod_{k=1}^{K} \exp(w_k^p \mathbf{v}_{k,l}^p) \quad \text{and} \quad \Phi_l^s(\mathbf{w}^s) = \exp_{\mu_l^s}(\sum_{k=1}^{K} w_k^s \mathbf{v}_{k,l}^s). \tag{2}$$

The registration is performed using a GMM-based technique proposed earlier [14]. In this iterative technique, soft-correspondences are established between surface of the model and the target that is represented by a point set. Assume that the *correspondance* function, $P(\mathbf{x}_n^l, \mathbf{y}_m)$, is defined for the nth point of the lth anatomy on the model, $\mathbf{x}_n^l$, and the mth point of the target, $\mathbf{y}_m$, and has a value between 0 and 1. The point set $\mathbf{Y}$ constitutes a partial surface of the vertebrae and is extracted from the ultrasound images as explained in the previous section. Additionally, the bone surface probability extracted from the ultrasound images is already integrated into the correspondence function.

The model is then instantiated and rigidly transformed to minimize the following objective function:

$$Q = \sum_{l=1}^{L} \sum_{m,n=1}^{M,N} P(\mathbf{x}_n^l | \mathbf{y}_m) \| \mathbf{y}_m - \big(\mathbf{R}\Phi(\mathbf{x}_n^l; \mathbf{w}^s, \mathbf{w}^p) + \mathbf{t}\big)\|^2 + \gamma^s \mathbf{\Gamma^s} \mathbf{w}^s + \gamma^p \mathbf{\Gamma^p} \mathbf{w}^p, \tag{3}$$

where the two latter terms are the regularization over the PGs weights, and matrices $\mathbf{\Gamma^s}$ and $\mathbf{\Gamma^p}$ are diagonal with elements $1/\lambda^s$ and $1/\lambda^p$, the corresponding eigenvalues of the shape and the pose PGs, respectively. The matrices $\mathbf{R}$ and $\mathbf{t}$ are the rotation and translation of the rigid transformation, respectively. The optimization is performed using the Quasi-Newton method.

Note that the objective function is minimized with respect to the points of the model that are visible in ultrasound volumes, i.e. laminae, articular processes and transverse processes of one side only (see Fig. 1b).

This is the key challenge. Once registered, the model is used later to estimate the location of the mid-sagittal plane. This is performed by fitting a plane to the tip of the spinous processes and most anterior point of the vertebral body.

3 Experiments and Results

3.1 Multi-vertebrae Shape+Pose Model

Training data for construction of the multi-vertebrae model consisted of lumbar (L1-L5) vertebrae of 32 patients, some with mild scolisis. Written informed consent was obtained from all patients. Manual CT segmentations were performed semi-automatically using ITK-SNAP. For each subject, three independent segmentations (performed by three different users) were averaged using majority voting to form the final segmentation, then triangulated using the marching cubes algorithm.

The statistical shape+pose model was reconstructed using the technique presented in the previous section. The first 10 modes capture 97% of pose variations and 70% of shape variations. The model is capable of reconstructing an unseen observation with distance error below 1.5 mm by using the first 10 modes of the variation.

3.2 Synthetic Data

To assess the performance of the registration of one side of the model to the corresponding ultrasound images in an ideal scenario, we constructed a synthetic data set using 32 CT scans and performed leave-one-out experiments. For each CT scan, the model is constructed using all other CT images and is registered to a surface extracted from one side of L1-L4 vertebrae of the target, including the laminae, articular processes and transverse processes. The surface error is then computed for the entire vertebrae and results in an RMS distance error of 2.2 ± 0.6 mm. Fig. 3 shows the distance error overlaid on the model. As expected, the registration error is smallest near the anatomy involved in the registration and increases further away. The registration error is largest around the spinous process since its shape is not correlated with laminae and transverse processes. This error is however not critical since the epidural space is not close to the spinous process and does not affect needle insertion. Interestingly, the error is equally distributed in the other regions, i.e. laminae and articular processes on the opposite side and vertebral body.

The registered model is then used to estimate the mid-sagittal plane and is compared against the mid-sagittal plane extracted from manual segmentation. The normals of the two planes differ by 4.4 ± 2.6 degrees, and the location of the epidural space in the registered model differs from the mid-sagittal plane of

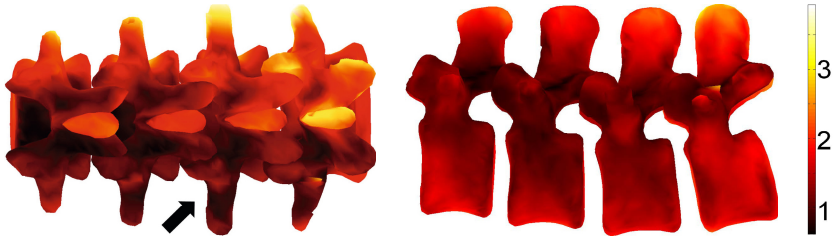

Fig. 3. Distance error overlaid on the model in the a) anterior-posterior and b) left-to-right view. The arrow points to the side used in the registration.

Table 1. The registration error of the model to the paramedian volume. Values are given as mean±std (mm).

		L1-L2	L2-L3	L3-L4	L4-L5	All
Registration side	RMS	2.0±0.3	3.0±1.7	2.5±0.9	3.0±1.1	2.6±1.2
	Haussdorf	3.7±1.0	6.8±4.3	4.6±2.7	5.1±2.8	5.0±3.1
Contra-lateral side	RMS	4.4±2.0	4.0±2.0	3.9±1.4	3.5±1.1	3.9±1.7
	Haussdorf	7.1±3.2	7.4±3.0	6.7±2.7	6.1±3.0	6.8±3.0

the manual segmentation by 1.3±1.2 mm. As we will mention in the Discussion, these errors effectively convey the ability to register the model using only a few features on only one side of the vertebral anatomy.

3.3 *In Vivo* Data

3D ultrasound volumes were captured by an expert sonographer using a Sonix Touch ultrasound machine (Ultrasonix, Medical Corp, Richmond, BC) with a curvilinear 3D transducer, operating at 3.3 MHz with depth of 7.0 cm. 80 frames were captured for each volume to have a 60 degree field of view. The 3D probe was tracked using an EM tracker (pciBird, Ascension Technology Corp., Burlington, VT, USA) and was calibrated using double N-wire phantom with an RMS error of 1.7 mm [3]. The purpose of tracking is only for validation of the model registration to the volumes on the contra-lateral side and for measurement of the true mid-sagittal plane.

Written consent was obtained from eight volunteers. Ultrasound volumes were acquired in the prone position. For each subject, the intervertebral levels were found using 2D ultrasound and were marked on the skin. A magnetic sensor (referred to as the reference) was attached on the skin above the T12 vertebra to track the patient's movement. We assumed that the spine curvature does not change during the entire scan. Four intervertebral levels (L1-L2, L2-L3, L3-L4, and L4-5) were scanned. Three volumes were acquired from each level (see Fig. 4), one paramedian volume from each side and one centered on the mid-sagittal plane (referred to as the *centered volume*). Note that bony features are

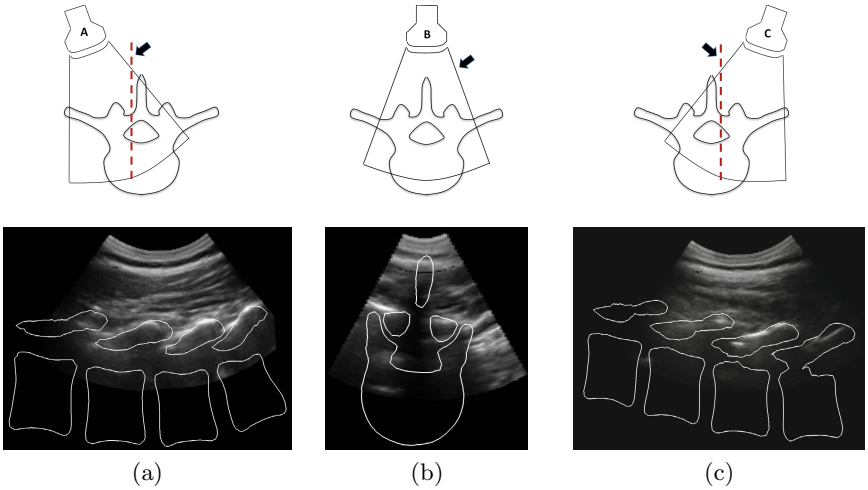

Fig. 4. Three volumes are acquired from each intervertebral level. Arrows show the plane visualized in each case. a) The model is registered to this paramedian volume (volume A). The red dashed line shows the sagittal slice of this volume shown together with the registered model. b) A transverse view of the centered volume (volume B) augmented with the registered model. c) A sagittal view of the contra-lateral volume (volume C) augmented with the registered model.

Table 2. Error between the two mid-sagittal planes, one estimated from the registered model, and one extracted from the centered 3D US volume. Distance is defined as the distance between two planes at the epidural depth.

	L1-L2	L2-L3	L3-L4	L4-L5	All
Normal (degree)	6.4±2.4	13.0±7.5	10.0±8.0	14.2±8.6	10.8±7.5
Distance (mm)	4.0±2.9	5.6±4.6	4.5±3.1	6.1±4.9	5.0±3.9

most visible in the paramedian volumes whereas the mid-sagittal plane is best detected in the centered volume. The ultrasound volumes were then transformed to the reference coordinate system using the position tracker measurements and calibration of the 3D ultrasound probe.

Registration Accuracy. The bone surfaces were manually extracted for each paramedian volume. The model was registered to one of the paramedian ultrasound volumes (e.g. volume A in Fig. 4). Examples of the registrations are shown in Fig. 5. The RMS and maximum (referred to as Haussdorf) distance between the manual segmentation of the ultrasound volume and the registered model are calculated and reported. We also reported the error between the same registered model and the paramedian ultrasound volumes acquired from the contra-lateral side (e.g. volume C in Fig. 4). Fig. 4a and 4c show an example of the registration. Results are given in Table 1. As expected the error is larger on the contra-lateral side, but remains below 4.4 mm.

Fig. 5. Examples of the registration. The multi-vertebrae model is capable of capturing different sizes, shapes and poses of vertebrae.

Detection of the Mid-Sagittal Plane. The mid-sagittal plane is detected by fitting a plane to the points acquired by marking the symmetric features of vertebral anatomy (i.e. laminae and transverse processes) and taking their average. The manually extracted plane is compared against the mid-sagittal plane extracted from the registered model. Similar to synthetic data, the angle between these two planes and their separation at the depth of the epidural space is reported. Results are given in Table 2. Fig. 4b shows an example of the registered model together with the centered volume.

4 Discussion and Conclusion

It is expected that the multi-vertebrae model will be used to augment the ultrasound image interpretation and to predict the mid-sagittal plane of the spine, but not replace the standard technique for epidural needle placement such as loss-of-resistance. In this pilot study, we have demonstrated that the errors for registering the model to single-sided ultrasound volumes of the human spine have an average of 2.6 mm on the registration side and 3.9 mm on average on the contra-lateral side.

The width of the ligamentum flavum covering the epidural space is reported to be 6.8±1.9 [11]. The epidural depth varies between patients, and increases with obesity. In our experiments, the maximum epidural depth was 47 mm. Given these numbers and referring to Fig. 1a, the safe needle insertion zone (represented by the gray area) confine the proper needle insertion to an angle of less than 8 degrees and 6.8 mm distance to the mid-sagittal plane. This suggests that the proposed method for mid-sagittal plane estimation has the potential for successful midline epidural injection. The results can be further improved by better edge enhancement in the ultrasound images and also using larger training set used for the construction of the model.

The current unoptimized MATLAB code requires 53 seconds to register the multi-vertebrae shape+pose model to 3D ultrasound images. Since the ultimate goal of this work is to visualize the ultrasound reslice augmented with the model in real-time, our future work involve optimizing the code in C++ to achieve clinically acceptable speeds.

Acknowledgments. This work is funded by the Natural Sciences and Engineering Research Council and Canadian Institutes for Health Research. The authors would also like to thank Victoria A. Lessoway for helping with data collection.

References

1. Belavy, D., Ruitenberg, M., Brijball, R.: Feasibility study of real-time three-/four-dimensional ultrasound for epidural catheter insertion. British Journal of Anaesthesia 107(3), 438–445 (2011)
2. Bossa, M., Olmos, S.: Multi-object statistical pose+shape models. In: IEEE International Symposium on Biomedical Imaging, ISBI, pp. 1204–1207 (2007)
3. Chen, T.K., Thurston, A.D., Ellis, R.E., Abolmaesumi, P.: A real-time freehand ultrasound calibration system with automatic accuracy feedback and control. Ultrasound in Medicine & Biology 35(1), 79–93 (2009)
4. Coq, G.L., Ducot, B., Benhamou, D.: Risk factors of inadequate pain relief during epidural analgesia for labour and deliver. Anaesthesia 45, 719–723 (1998)
5. Duta, N., Sonka, M.: Segmentation and interpretation of MR brain images. an improved active shape model. IEEE TMI 17(6), 1049–1062 (1998)
6. Fletcher, P., Lu, C., Joshi, S.: Statistics of shape via principal geodesic analysis on lie groups. In: IEEE CVPR, vol. 1, pp. 95–101 (2003)
7. Foroughi, P., Boctor, E., Swartz, M., et al.: 2-D ultrasound bone segmentation using dynamic programming. In: IEEE Ultras Symp., pp. 2523–2526 (2007)
8. Grau, T., Bartusseck, E., Conradi, R., et al.: Ultrasound imaging improves learning curves in obstetric epidural anesthesia: a preliminary study. Canadian Journal of Anesthesia 50(10), 1047–1050 (2003)
9. Khallaghi, S., et al.: Registration of a statistical shape model of the lumbar spine to 3D ultrasound images. In: Jiang, T., Navab, N., Pluim, J.P.W., Viergever, M.A. (eds.) MICCAI 2010, Part II. LNCS, vol. 6362, pp. 68–75. Springer, Heidelberg (2010)
10. Lu, C., Pizer, S.M., Joshi, S., Jeong, J.: Statistical multi-object shape models. International Journal of Computer Vision 75(3), 387–404 (2007)
11. Nickalls, R., Kokri, M.: The width of the posterior epidural space in obstetric patients. Anaesthesia 41(4), 432–433 (1986)
12. Okada, T., Yokota, K., Hori, M., Nakamoto, M., Nakamura, H., Sato, Y.: Construction of hierarchical multi-organ statistical atlases and their application to multi-organ segmentation from CT images. In: Metaxas, D., Axel, L., Fichtinger, G., Székely, G. (eds.) MICCAI 2008, Part I. LNCS, vol. 5241, pp. 502–509. Springer, Heidelberg (2008)
13. Rasoulian, A., Abolmaesumi, P., Rohling, R., Kamani, A., Charles, L., Lessoway, V.: Porcine thoracic epidural depth measurement using 3D ultrasound resliced images. In: Canadian Anesthesiologists Society Annual Meeting (2011)
14. Rasoulian, A., Rohling, R., Abolmaesumi, P.: Group-wise registration of point sets for statistical shape models. IEEE TMI 31(11), 2025–2034 (2012)
15. Rasoulian, A., Rohling, R., Abolmaesumi, P.: Probabilistic registration of an unbiased statistical shape model to ultrasound images of the spine. In: SPIE Medical Imaging, vol. 8316, pp. 83161P–1 (2012)
16. Sprigge, J., Harper, S.: Accidental dural puncture and post dural puncture headache in obstetric anaesthesia: presentation and management: A 23-year survey in a district general hospital. Anaesthesia 63(1), 36–43 (2007)
17. Steiner, H., Staudach, A., Spitzer, D., Schaffer, H.: Diagnostic techniques: Three-dimensional ultrasound in obstetrics and gynaecology: technique, possibilities and limitations. Human Reproduction 9(9), 1773–1778 (1994)